

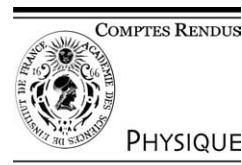


ELSEVIER

Available online at www.sciencedirect.com

SCIENCE @ DIRECT®

C. R. Physique 5 (2004) 297–304



COMPTES RENDUS
PHYSIQUE

Highly polarized nuclear spin systems and dipolar interactions in NMR/Systèmes de spins nucléaires fortement polarisés et interactions dipolaires en RMN

^{129}Xe NMR – highly polarized thin films

Peter Gerhard, Matthias Koch, Heinz J. Jänsch

Department of Physics and Center for Materials Science, Philipps Universität Marburg, 35032 Marburg, Germany

Available online 17 April 2004

Presented by Guy Laval

Abstract

We studied the macroscopic effects of nuclear magnetization. Highly polarized xenon is often used to increase the sensitivity in NMR investigations of porous media, diluted liquids or for imaging in the gas phase. In the condensed phase, however, highly nuclear spin polarized xenon also possesses a sizable magnetization due to the nuclear spin density. This results in an additional magnetic field, that is used to measure the polarization of the sample, when only the particle density is known. Here we find $P_z \approx 0.8$ corresponding to a spin temperature of 0.5 mK. We use isotopically enriched xenon with a ^{129}Xe abundance of 0.71. At high abundance of ^{129}Xe and high nuclear polarization the dipolar linewidth is considerably reduced. We find for small angle excitation a reduction from 650 Hz to 400 Hz. We investigate this using a thin film geometry. The susceptibility effects of the substrate and the Xe film are treated. The macroscopic angle between the normal of the film and the external field strongly changes the polarization induced line shift and line width. The first follows an expected $\cos^2\theta$ dependence with an understood amplitude the latter however is not understood up to now. Relaxation of ^{129}Xe in the condensed film is observed to be $T_1 = 15 \pm 1.8$ min, much faster than expected. **To cite this article: P. Gerhard et al., C. R. Physique 5 (2004).**

© 2004 Académie des sciences. Published by Elsevier SAS. All rights reserved.

Résumé

RMN du ^{129}Xe – films fins hautement polarisés. Nous étudions les effets macroscopiques de l'aimantation nucléaire. Le xénon fortement polarisé est souvent utilisé pour accroître la sensibilité d'exploration par RMN de poreux, de liquides dilués ou pour effectuer l'imagerie en phase gazeuse. Toutefois, en phase condensée les échantillons de xénon, dont le spin nucléaire est fortement polarisé, disposent d'une aimantation dépendante de la densité de spins nucléaires. Ceci induit un champ magnétique supplémentaire, qui est utilisé afin de mesurer la polarisation de l'échantillon, quand la densité est connue. Nous trouvons ici $P_z \approx 0,8$ ce qui correspond à une température de spin de 0,5 mK. Nous utilisons du xénon contenant une teneur isotopique de 0,71 en ^{129}Xe . Pour des hautes abondances isotopiques en ^{129}Xe et pour des fortes polarisations nucléaires, la largeur de raie dipolaire est considérablement réduite. Nous trouvons pour de faibles angles d'excitation une réduction de 650 à 400 Hz. Nous étudions ce phénomène en utilisant la géométrie d'un film mince et en prenant en compte l'effet de la susceptibilité du substrat et celle du film de xénon. L'angle macroscopique entre la normale au film et le champ extérieur affecte fortement, à travers l'effet de la polarisation, le décalage fréquentiel et la largeur de la raie. La fréquence de résonance varie effectivement suivant la loi en $\cos^2\theta$ avec une amplitude attendue ; cependant la dépendance de la largeur de raie en fonction de θ reste incomprise. L'étude de la relaxation du ^{129}Xe dans le film condensé permet de mesurer $T_1 = 15 \pm 1,8$ min, une valeur bien plus courte qu'attendue. **Pour citer cet article : P. Gerhard et al., C. R. Physique 5 (2004).**

© 2004 Académie des sciences. Published by Elsevier SAS. All rights reserved.

Keywords: Nuclear magnetic resonance (NMR); ^{129}Xe ; Optical pumping; Dipolar line width

Mots-clés : Résonance Magnétique Nucléaire (RMN) ; ^{129}Xe ; Pompage optique ; Largeur de raie dipolaire

E-mail address: heinz.jaensch@physik.uni-marburg.de (H.J. Jänsch).

1631-0705/\$ – see front matter © 2004 Académie des sciences. Published by Elsevier SAS. All rights reserved.

doi:10.1016/j.crhy.2004.02.007

1. Introduction

Xenon has been used to study large area surfaces for quite some time [1–5]. The high sensibility of ^{129}Xe towards its physical environment, i.e. its large chemical shift range in physisorption, makes it especially suited for this task. The sensitivity of the NMR studies has been greatly increased by using laser-polarized, so called hyperpolarized, ^{129}Xe [5]. Smaller area substrates, diluted systems as dissolved Xe or gas filled volumes as in the lung became accessible to ^{129}Xe -NMR. The present results are part of an endeavor to study the 1 cm^2 area of a highly polished, oriented and cleaned metal single crystal surface. First results have been obtained on ^{129}Xe adsorbed on CO- or CH_3C - coated Ir(111) [6]. Chemical shift differences between the two preparations demonstrate the usefulness of ^{129}Xe atom as a probe. Highly polarized adsorbates were necessary to overcome the extreme lack of sensitivity in that system.

Using spin exchange optical pumping at low gas pressures a ^{129}Xe -polarization between 0.4 and 0.8 is achieved on a regular basis. The metal crystal can be cooled below 30 K so that even in a ultra high vacuum environment stable films of xenon can be grown. The crystal can be rotated within the magnet such that the surface normal is varied from parallel to perpendicular with respect to B_0 . Here we present NMR results obtained from these films of highly polarized ^{129}Xe -nuclei. The absolute polarization has been determined. Polarization dependent line shifts and line widths have been measured. Both show distinct angular dependences. The susceptibility effects of the metallic bulk and the xenon films have been measured and treated theoretically to determine the contribution to chemical shift anisotropy measurements. Furthermore, the spin lattice relaxation time T_1 has been determined.

2. Experimental set-up

The experimental apparatus has been described in more detail elsewhere [7–9]. An ultra high vacuum (UHV) chamber is connected to an NMR setup and to an optical pumping system. The base pressure of the UHV system is 5×10^{-10} mbar. The chamber contains the crystal, its support structure for heating, cooling, and positioning, a sputter gun, a quadrupole mass spectrometer (QMS) and a gas handling manifold. The temperature is measured by a chromel/constantan (type E) thermocouple. At low enough temperatures ≈ 80 K both materials become ferromagnetic. Thin wires are mandatory in order to keep magnetic distortions due to the ferromagnetic wires well within our experimental line width. The $75\ \mu\text{m}$ thin wires are spot welded to the backside of the crystal. The NMR spectrometer is essentially home built and consists of a single channel irradiation and detection system. We use an electromagnet with a 1.98 T field that gives a ^{129}Xe resonance frequency of 23.275 MHz. The spin of ^{129}Xe is $1/2$, the spin of ^{131}Xe is 1. Due to quadrupolar interaction the T_1 -times of latter isotope is much smaller then of ^{129}Xe . Therefore the xenon used is isotopically enriched to 71% ^{129}Xe and deriched in ^{131}Xe content to below 1% (provider URENCO). The rest (all other isotopes) has spin zero.

The hyperpolarized xenon is produced in a setup a few meters away from the NMR spectrometer. It is transferred from the optical pumping to the UHV-NMR-setup through a 5 m long tube, made from PTFE a teflon variant. The xenon is stored in frozen form in a reservoir inside the gap of the magnet. It is dosed onto the crystal by using its own vapor pressure. Slow dose rates of 4 to 40 monolayers per second (ML/s) are achieved by leaving the reservoir at 77 K or 87 K (boiling points of liquid nitrogen and argon, respectively) [10]. Removing the coolant results in a burst of xenon gas for a few seconds which builds a film of about 1000 to 2000 monolayers thickness when the crystal is well below 60 K.

In building the xenon handling system care was taken not to have contact with materials that destroy the xenon polarization quickly. Tests were made which materials were tolerable in contact with xenon. For this the polarized gas was streaming across samples of 1 or 2 cm^2 of various substances and the polarization determined before and after [11]. All materials were at room temperature. It was found that Cu, Ag, Au, Al, Mo, Ta, W, Pt-Ir, soft and hard solder alloy and also Chromel are permissible (no observed reduction of P_z). Brass which is nominally iron free often contains some iron, so that it can be slightly magnetized. Such samples were also permissible. Losses in excess of 90% were found in: iron in various states of cleanliness, stainless steel (2 out of three samples) and also Alumel thermocouple wire. Intermediate losses (in % lost) occurred with stainless steel (60–70%; 1 of three samples), iron under 2 layers of teflon tape (60%). A sprayed lacquer layer directly on iron samples did not help. The inhomogeneous field of a strong small permanent magnet placed outside the glass tube through which the xenon flows reduced the polarization by 50%. All of these values can only be a guide in selecting appropriate materials for production or transport of polarized xenon gas. A rule of thumb is that non-metals and metals are permissible, as long as they have no ferromagnetic material in them. All tests above were performed with gas flow meaning short contact times.

With the above in mind, the optical pumping setup has been made from glass and teflon. Differentially pumped copper connectors are used to link the PTFE tube to the optical pumping setup and the UHV gas handling system. The latter made from glass. Differentially pumped glass stem valves (with viton o-rings) are employed in the xenon dosing manifold.

3. Results and discussion

3.1. Pulse angle and polarization measurement

The crystal is a solid disk of iridium metal with a diameter of 10.1 mm and a thickness of 2.1 mm. It is supported by metallic wires and held in the NMR solenoidal coil (diameter 25 mm, length 20 mm). Surprisingly does the insertion of the crystal into the coil not change the 50Ω tuning (below 1Ω change). The pulse angle however must be determined when the crystal is inserted into the coil. For this purpose we prepare a film of highly polarized xenon (on the crystal) and expose it to a series of rf-pulses much shorter than a 90° pulse. Nevertheless, strong signals are obtained at the position of the xenon bulk 320 ppm shifted from the gas line. Fig. 1 shows obtained resonance lines for a highly polarized sample: (a) at the beginning of the series; and (b) for low polarization at the end. In Fig. 2(a) the amplitudes are shown. They show a dependence on the pulse number n like $(\cos \theta)^n$ which gives the pulse angle $\theta = 19^\circ$ in this case. The slightly different behavior of the initial few points is not completely understood. We use the middle section of the series to determine the pulse angle. Fig. 2(b) shows the behavior of the spectral line position. The polarization dependent line shift reaches up to 269 Hz. In the analysis we follow the one given for highly polarized ^3He films [12,13]

$$\Delta\nu = A(3\cos^2\theta - 1)\frac{\gamma}{2\pi}\mu_0M. \tag{1}$$

Here $A = -1/2$ is a geometry dependent factor that also includes the fact that the nucleus producing the additional field is the one in resonance. θ is the angle between the crystal surface normal, i.e. the film normal, and the external field. The magnetization is the product $M = -\mu\rho\eta P_z$, namely the nuclear moment, μ , the density, n , the isotopic abundance, η , and the

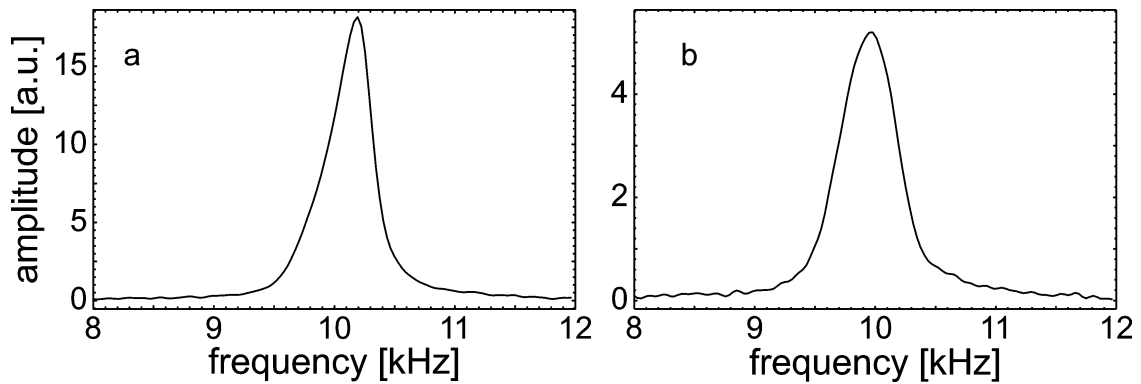


Fig. 1. A typical bulk resonance line at (a) high and (b) low polarization. The film orientation was 90° .

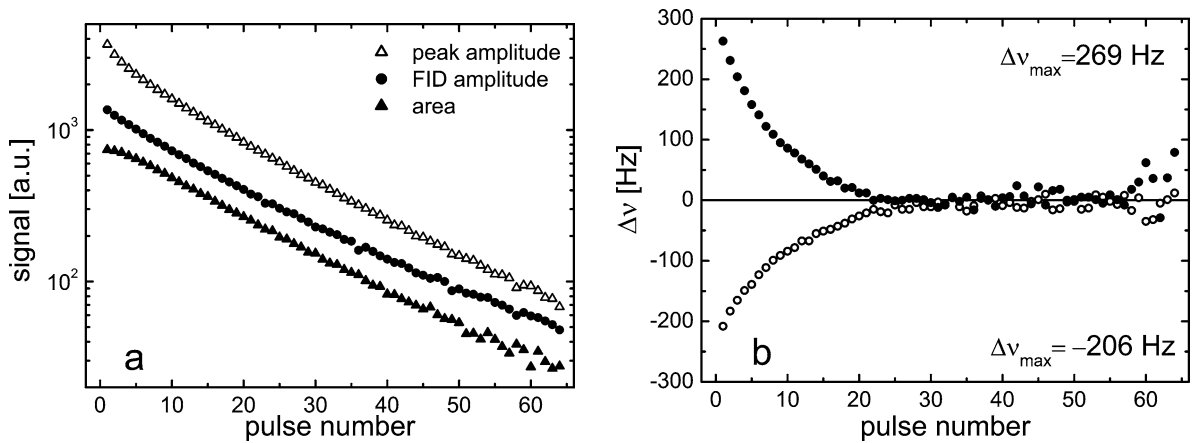


Fig. 2. (a) The amplitude of the peak height, the FID and the peak area in the NMR spectra when a film is measured with a sequence of small angle excitation pulses ($\approx 20^\circ$ in this case). (b) The line shift in such a measurement with initially positive or negative polarization. A shift of 269 Hz gives $P_z = 0.81$ (see text). The sample orientation is $\theta = 90^\circ$, i.e. the magnetic field lies in the plane of the film.

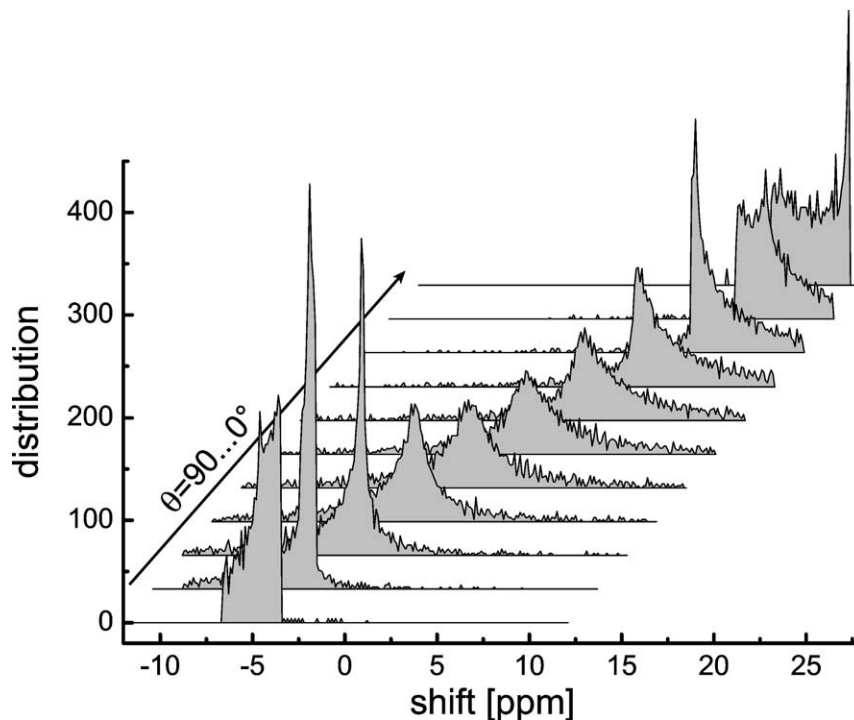


Fig. 3. Results of a numerical simulation of the susceptibility effects of the iridium crystal are shown. For surface orientations from 0 to 90 degrees the distribution of B-fields just outside the bulk is given in histogram form.

nuclear polarization, P_z (all of ^{129}Xe). At 58 K we use a density of $\rho = 1.603 \times 10^{28} \text{ m}^{-3}$ [14]. All together the polarization follows $P_z = \Delta\nu/333 \text{ Hz}$ giving $P_z = 0.81$ for the positive shift in Fig. 2(b) and -0.62 for the negative one. This corresponds to spin temperatures of 0.5 mK and -0.8 mK respectively.

3.2. Line width and shift: susceptibility effects

Line width estimates are always quite difficult especially when one has to consider a non-ideal sample geometry. The FWHM dipolar line width, $\Delta_2(0)$, at small (≈ 0) polarization is given by Yen and Norberg [15]. With natural abundance $\Delta_2(0) = 353 \text{ Hz}$ at 103 K. For our case ^{131}Xe is 'deriched' below 1%, so its contribution can be ignored. The 71% ^{129}Xe abundance however lead to $\Delta_2(0) = 540 \text{ Hz}$ at 103 K and 561 Hz at 50 K. The xenon film condenses on one crystal face (towards the xenon inlet). The film has a thickness of $\approx 1 \mu\text{m}$ and a diameter of 1 cm. An infinite film is a good approximation in this case. The susceptibility (SI units) of the xenon bulk is $\chi_{\text{Xe}} = -15 \times 10^{-6}$ [16]. Including the Lorentz sphere the angle dependent shift [17] is $\Delta\nu/\nu_0 = -\chi_{\text{Xe}}(3\cos^2\theta - 1)/3$, giving a shift of +10 ppm and -5 ppm at 0° and 90° respectively.

The substrate iridium crystal is paramagnetic with $\chi_{\text{Ir}} = +38 \times 10^{-6}$ [16]. The geometry, however, is far from ideal, with a diameter only 5 times the thickness. The effect on the local field has to be treated numerically. This has been done by integrating the magnetization through a surface integral over the idealized cylindrical sample geometry [18]. The result is a magnetic potential, the negative gradient of which is the desired H field. Only the relevant z -component has been calculated. The xenon sits on the surface of the iridium disk only. To obtain the field distribution, the surface has been sampled in a two-dimensional grid with 0.1 mm spacing. Fig. 3 shows the result in a histogram form for angles from 0° to 90° . The noise in the histogram comes from the finite sampling but the unusual overall shapes with sometimes sharp features come from the sample geometry where cusps occur in the field distribution. The second moment or the width of the distributions is between 2–4 ppm. The centroid follows very closely $\Delta\nu/\nu_0 = a(3\cos^2\theta - 1)/3 + b$ with $a = 13.6 \pm 0.2 \text{ ppm}$ and $b = -0.1 \pm 0.1 \text{ ppm}$.

The shifts due to iridium, although paramagnetic, are of the same sign as the shifts due to the diamagnetic xenon bulk. The difference being, of course, that the xenon nuclei are *inside* the xenon bulk and *outside* of the iridium. Altogether the angle dependent shift follows $\Delta\nu/\nu_0 = (28.6 \pm 0.2 \text{ ppm})(3\cos^2\theta - 1)/3$. The offset has been omitted since it cannot be determined experimentally in our setup. Fig. 4 shows the result of a shift measurement at low nuclear polarisation. The fit to the data gives an amplitude $27.2 \pm 1.8 \text{ ppm}$, in good agreement with the theoretical estimate. With these data and the analysis the substrate dependent part of the angular shift is well understood and can be taken into account quantitatively, where ever necessary. The

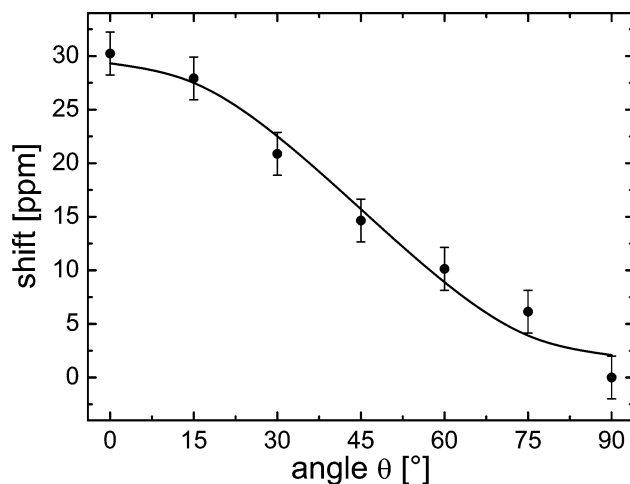


Fig. 4. The experimental angle dependent line shift of a xenon film at low polarization is shown. The fit to $A \times (3 \cos^2 \theta - 1)/3$ yields an amplitude of $A = 27.2 \pm 1.8$ ppm.

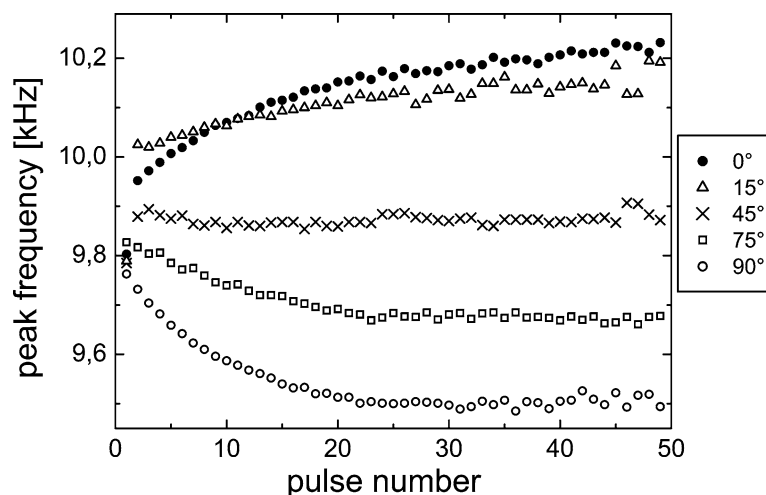


Fig. 5. Line shift measurements using small angle excitation. For several film orientations the resonance line position is given as a function of the excitation pulse number. A strong dependence is visible at low pulse numbers (high polarization). The susceptibility effects are seen at high pulse numbers (low polarization). The polarization dependent effects are of opposite sign going from 0° to 90° .

line width contribution from the bulk susceptibility is only 2–4 ppm, justifying the selection of iridium as a bulk. Assuming the same geometry one would expect for substrates such as Ru(001), Pt(111), and Pd(111) angular shift amplitudes (all in ppm and substrate contribution only) of 23.4, 99.8, and 288 respectively. For the line width, the contribution would be (also in ppm) 3.5–7, 21–42, and 42–84 respectively. Especially for Pd the size of the effect becomes almost prohibitively large when one thinks of monolayer experiments.

3.3. Line shift and width: angular effects

As already discussed in Section 3.1 the line shift effects are due to the nuclear magnetism. They are quite sizable and easily measured in a dense, highly polarized sample. The results seen in Fig. 2 were obtained at 90° sample orientation. Fig. 5 shows the results of several experiments each with small pulse angle excitation but different orientation of the surface towards the external field. At high pulse numbers (low polarization) the shift is determined by the susceptibility effects. At low pulse numbers, i.e. high polarization, strong polarization induced shifts are visible. The sign of the shift is opposite for 0° and 90° as expected from Eq. (1). Quantitative agreement could not be reached, since the samples have a slightly varying initial polarization (seen in the very first data point in Fig. 2). Additionally, the rotation of the sample seems to play a role not understood yet.

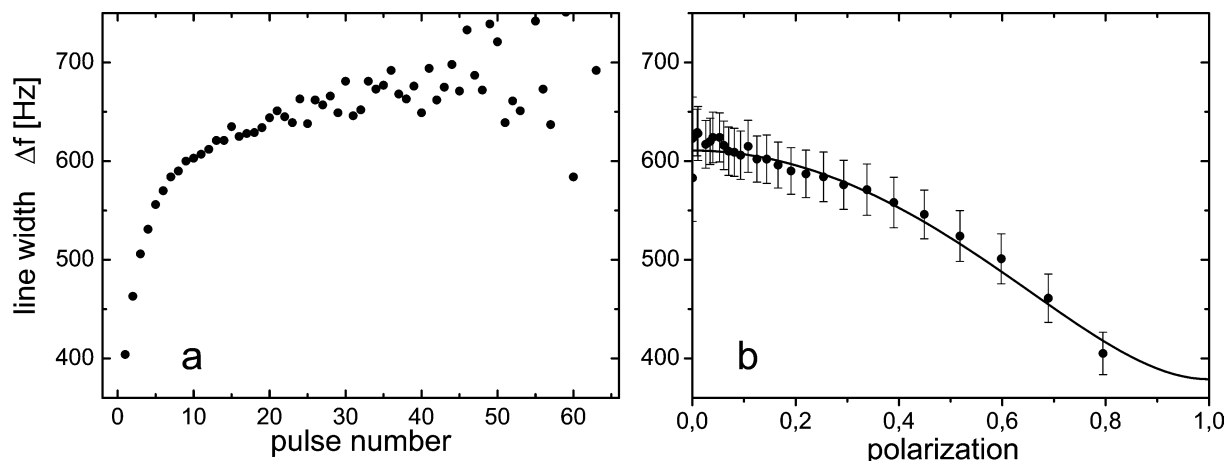


Fig. 6. (a) The FWHM line width of a small angle excitation measurement as a function of the excitation pulse number. Orientation is $\theta = 90^\circ$ (b) The same data as in (a) but plotted against the sample polarization as determined by the line shift. The error bars indicate an estimate of the overall systematic error. At low polarization not all points are shown. The solid line is a fit using $\Delta f = \sqrt{\Delta_{\text{off}}^2 + (\Delta_2(0)(1 - P_z^2))^2}$ (see text).

For each measurement the xenon film is prepared at 90° followed by a single pulse excitation to determine the polarization of that particular film. Then the sample is rotated to its final position where the multipulse experiment proceeds. Spin lattice relaxation during the rotation is unlikely since the time for the rotation is less than one minute and $T_1 \approx 15$ min as discussed in Section 3.4.

Apart from the line shift effect there is a substantial reduction of the line width due to the nuclear polarization. Fig. 6(a) shows this clearly. It is again a small angle excitation experiment and the line width Δf (FWHM) is given as a function of the excitation pulse number. As the polarization decreases with the pulse number the line width reduction quickly ceases. The effect should follow $\Delta_2(P_z) = \Delta_2(0)(1 - P_z^2)$ [19]. In Fig. 6(b) the line width is therefore plotted versus P_z . The data is fitted with $\sqrt{\Delta_{\text{off}}^2 + (\Delta_2(P_z))^2}$ giving $\Delta_{\text{off}} = 380$ Hz and $\Delta_2(0) = 490$ Hz. Here geometric averaging is assumed. Δ_{off} resembles the non-dipolar line width contributions, like from paramagnetic impurities, vacancies, remaining ^{131}Xe nuclei, or field inhomogeneity. The $\Delta_2(0)$ should be the FWHM dipolar line width value discussed in Section 3.2, namely 561 Hz (50 K). Reasons for the somewhat smaller $\Delta_2(0)$ are not clear.

The angular behavior of the line width effect is not completely understood. Fig. 7 shows this orientation dependence of the line width reduction due to high nuclear polarization. The line width is given as a function of the pulse number in a small angle excitation measurement. At 90° and 75° there is still a sizable line width reduction at high polarization (small pulse numbers). The measurement at 0° shows no such effect at all. The data at 0° is representative of measurements at 60° , 45° , 30° , and 15° which also show no polarization dependence of the line width at all.

The resonance lines at high polarization are somewhat asymmetric as is predicted [19]. Typical lines at high (a) and low (b) polarization are shown in Fig. 1.

3.4. Relaxation measurements

The longitudinal relaxation time has also been determined in a small pulse angle experiment. After preparation of the film the sample was excited by 25 pulses each 30 s apart followed by 35 pulses each 0.2 s apart. The peak height of the measured lines is shown in Fig. 8. On the log scale two slopes are visible. The higher slope at low pulse numbers contains the effect of T_1 and of the pulse angle. The lower slope at the higher pulse numbers results from the pulse angle only. Analysis of the data gives a $T_1 = 15 \pm 1.8$ min. This is a surprisingly low time when compared to the several hours seen in other experiments [20]. A possible explanation could be spin diffusion towards fast relaxing sites. Those may be paramagnetic contaminants as in oxygen molecules or the metal electrons of the iridium substrate. T_1 was measured with the film condensed on CO covered Ir and on the Ir itself. No differences were found. The first xenon layer on the metal is different enough from the Xe in the bulk to serve as an effective spin diffusion barrier. The contaminants have been discussed in [9,21] to explain our relatively fast relaxation in the reservoir (10–20 min) where the xenon is frozen for storage. The similarity to the film T_1 is striking but could be accidental. An oxygen contamination might also be responsible for the relatively large remaining line width even at very high nuclear polarization.

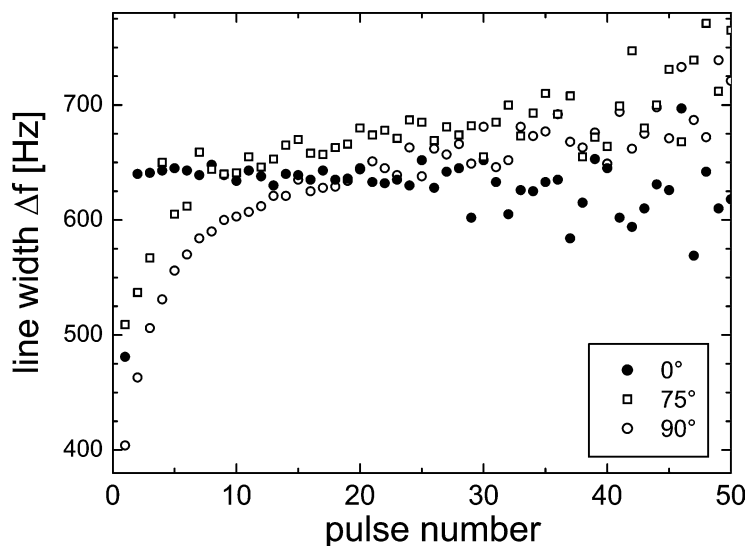


Fig. 7. Film orientation dependence of the line width reduction due to high nuclear polarization. The line width is given as a function of the pulse number in small angle excitation measurements. At 90° and 75° there is a strong line width reduction at high polarization (small pulse numbers). At 0° no such effect is present at all, neither is it for angles of 60° or below. The polarization of the film was checked at 90° for every orientation using the first excitation pulse. A small line width difference with angle is present at high pulse numbers (≈ 70 Hz). It probably reflects field inhomogeneities.

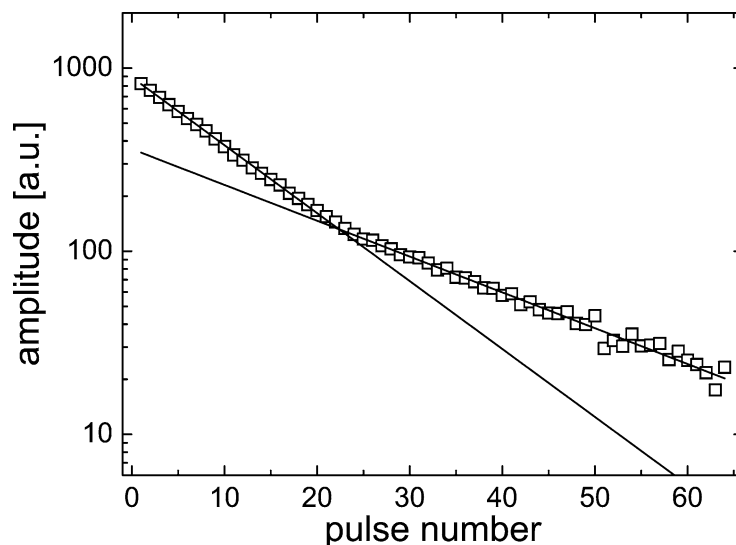


Fig. 8. T_1 measurement. The peak height in a small angle excitation experiment is shown as a function of the pulse number. Below pulse number 25 there is a 30 s delay time between pulses. At higher pulse number this delay is 0.2 s. $T_1 = 15 \pm 1.8$ min can be extracted from this.

4. Conclusion

The dipolar effect on the line position has been very useful in the determination of the nuclear polarization in our NMR setup that is geared towards surface science. The ultra high vacuum equipment cannot be easily replaced by a standard sample which might usually be used to determine P_z . The line width effects are quite strong but are not very well understood up to now. Possible contaminants have been discussed. The very high nuclear polarization of 0.8 is achieved not by extraordinary low sample temperatures but by a strike of light. Therefore one might replace in Chapter 5 of [19]: “*The spin who came in from the cold!*” and say now: *The spin who came in from the fire!*

Acknowledgement

The authors wish to thank the Deutsche Forschungsgemeinschaft (DFG), Bonn, for financial support. We also thank D. Fick for many fruitful discussions and continuous support.

References

- [1] T. Ito, J. Fraissard, ^{129}Xe NMR study of xenon adsorbed on Y zeolites, *J. Chem. Phys.* 76 (1982) 5225–5229.
- [2] J.L. Bonardet, J. Fraissard, A. Gedeon, M.A. Springuel-Huet, Nuclear magnetic resonance of physisorbed ^{129}Xe used as a probe to investigate porous solids, *Catal. Rev.* 41 (1999) 115–225.
- [3] J. Fraissard, NMR studies of supported metal catalysts, *Catalysis Today* 51 (1999) 481–499.
- [4] T. Pietraß, A. Bifone, A. Pines, Adsorption properties of porous silicon characterized by optically enhanced ^{129}Xe NMR spectroscopy, *Surf. Sci. Lett.* 334 (1995) L730–L734.
- [5] B.M. Goodson, Nuclear magnetic resonance of laser-polarized noble gases in molecules, materials, and organisms, *J. Magn. Reson.* 155 (2002) 157–216.
- [6] H.J. Jänsch, P. Gerhard, M. Koch, D. Stahl, ^{129}Xe chemical shift measurements on a single crystal surface, *Chem. Phys. Lett.* 372 (2003) 325–330.
- [7] H.J. Jänsch, T. Hof, U. Ruth, J. Schmidt, D. Stahl, D. Fick, NMR of surfaces: sub-monolayer sensitivity with hyperpolarized ^{129}Xe , *Chem. Phys. Lett.* 296 (1998) 146–150.
- [8] U. Ruth, T. Hof, J. Schmidt, D. Fick, H.J. Jänsch, Production of nitrogen-free, hyperpolarized ^{129}Xe gas, *Appl. Phys. B* 68 (1999) 93–97.
- [9] D. Stahl, W. Mannstadt, P. Gerhard, M. Koch, H.J. Jänsch, T_1 -relaxation of ^{129}Xe on metal single crystal surfaces – multilayer experiments on iridium and monolayer considerations, *J. Magn. Reson.* 159 (2002) 1–12.
- [10] P.B. Gerhard, Konventionelle Puls-NMR an ^{129}Xe auf Einkristalloberflächen, Ph.D. thesis, Philipps-Universität, Marburg, 2003.
- [11] U. Ruth, Präparation höchstpolarisierten Xenongases für neue Anwendungen der NMR-Spektroskopie, Master's thesis, Philipps-Universität, Marburg, 1998.
- [12] D. Canet, *NMR – Konzepte und Methoden*, Springer-Verlag, Berlin, 1994.
- [13] G. Tastevin, Helium–trois polarise: ondes de spin et liquefaction du gaz, Ph.D. thesis, Université de Paris, Paris, 1987.
- [14] D.R. Sears, H.P. Klug, Density and expansivity of solid xenon, *J. Chem. Phys.* 37 (1962) 3002–3006.
- [15] W.M. Yen, R.E. Norberg, Nuclear magnetic resonance of ^{129}Xe in solid and liquid xenon, *Phys. Rev.* 131 (1963) 269–275.
- [16] R.C. Weast (Ed.), *CRC Handbook of Chemistry and Physics*, 57 edition, CRC Press, Cleveland, OH, 1976.
- [17] J.R. Zimmerman, M.R. Foster, Standardization of N.M.R. high resolution spectra, *J. Phys. Chem.* 61 (1957) 282.
- [18] G. Mozurkewich, H.I. Ringermacher, D.I. Bolef, Effect of demagnetization on magnetic resonance line shapes in bulk samples: Application to tungsten, *Phys. Rev. B* 20 (1979) 33–38.
- [19] A. Abragam, M. Goldman, Nuclear Magnetism: Order and Disorder, in: *Int. Ser. Monographs Phys.*, Clarendon Press, Oxford, 1982.
- [20] G.D. Cates, D.R. Benton, M. Gatzke, W. Happer, K.C. Hasson, N.R. Newbury, Laser production of large nuclear-spin polarization in frozen xenon, *Phys. Rev. Lett.* 65 (1990) 2591–2594.
- [21] D. Stahl, NMR an hyperpolarisiertem ^{129}Xe auf Einkristalloberflächen, Ph.D. thesis, Philipps-Universität, Marburg, 2000.